Scientific Research Publishing

Optics and Photonics Journal, 2022, 12, 147-155
https://www.scirp.org/journal/opj
ISSN Online: 2160-889X
ISSN Print: 2160-8881

Optimization of Crystal Structure Based on Experimentally Obtained XRD Patterns for Fluorescence of Sm^{3+}-Doped TiO_2 Thin Films by Machine Learning

Yuri Tamamoto[1], Mariko Murayama[1,2], Xiwei Zhao[1,3]

[1]Department of Physics, Tokyo University of Science, Tokyo, Japan
[2]Research Institute of Industrial Technology, Toyo University, Saitama, Japan
[3]Department of Materials Science and Engineering, Xihua University, Chengdu, China
Email: xwzhao@rs.tus.ac.jp

How to cite this paper: Tamamoto, Y., Murayama, M. and Zhao, X.W. (2022) Optimization of Crystal Structure Based on Experimentally Obtained XRD Patterns for Fluorescence of Sm^{3+}-Doped TiO_2 Thin Films by Machine Learning. *Optics and Photonics Journal*, **12**, 147-155.
https://doi.org/10.4236/opj.2022.126011

Received: May 17, 2022
Accepted: June 25, 2022
Published: June 28, 2022

Abstract

The luminescence intensity of rare-earth ion-doped luminescent materials is closely related to the configuration of the anions around the rare-earth ions added to the host material and the lattice defects. And it is expected that this information will be reflected in the XRD pattern. In this study, the luminescence data and XRD patterns of Sm-doped TiO_2 accumulated by our group are used to construct a model to predict the integrated luminescence intensity. The model was confirmed to be able to predict the integrated luminescence intensity with high accuracy. Furthermore, we found that the integrated luminescence intensity of this system is closely related to the change in the position of the peak on the (200) plane of TiO_2.

Keywords

Machine Learning, Phosphor, TiO_2

1. Introduction

Rare-earth (RE) ion-doped phosphors have attracted much attention in applications such as solar cells [1] [2] [3], photocatalysts [4], and white Light-Emitting Diodes (W-LEDs) [5] [6], displays and temperature sensing [7], because they exhibit sharp and intense luminescence in the visible and near-infrared wavelength regions. Since the 4f inner-shell transition of rare-earth ions is generally prohibited, host materials that relax the selection rule are candidates for utilizing the luminescence phenomenon derived from this transition [8]. Of these, rutile

and anatase types of titanium oxide (TiO_2) thin films are the most likely candidates. In our group's previous research [9] [10] [11] [12] [13], we found that the best way to increase the luminescence derived from RE ions is to add them to anatase TiO_2 (A-TiO_2), and when Sm^{3+} or Nd^{3+} ions are added to TiO_2, they replace the Ti sites and are incorporated into the TiO_2 matrix. According to a detailed X-ray absorption fine structure (XAFS) analysis, the difference in luminescence is explained by the change in the ligand structure of the REs when added to the rutile and anatase crystal lattices. When adding to the rutile, the distances between the surrounding six oxygen ions are equal, but when adding to anatase, the sample showed strong luminescence because the six-fold oxygen ions are distinguished by four oxygen ions (O_4) and two oxygen ions (O_2). The difference in distance between these two types of oxygen ions and RE ions is large, which enhances luminescence. Based on the Judd-Ofelt theory [14] [15], the ligand structure surrounding the REs determines the spontaneous emission rate of the REs, which may be interpreted as an increase in the spontaneous emission rate due to the low symmetry induced in anatase. In addition, since the branching rate of anatase luminescence varies little between samples, it may be closely related to the increase in the population of low-symmetry ligand structures that enhance or induce this luminescence. We know that symmetry that maximizes luminescence can be obtained by annealing Sm-doped TiO_2 formed on a Si (100) substrate at 700˚C - 800˚C in an oxygen atmosphere. However, with this information, it is necessary to repeat the experiment again to find the optimum parameters when the board is changed. In addition, there is still a degree of freedom in selecting the board, so it is not sufficient information for establishing new measures. In this study, we aim to propose a strategy to produce materials with high luminescence intensity from XRD data. For this purpose, we used LASSO regression one of the machine learning algorithms [16], to predict the integrated luminescence intensity using the experimentally obtained XRD patterns as explanatory variables.

2. Experimental Methods

Sm-doped TiO_2 thin films were deposited on Si (100) substrate by laser ablation using a YAG laser (λ = 355 nm, 1 W/cm^2). The crystal structure of TiO_2 can be selected between anatase and rutile forms by carefully manipulating the oxygen partial pressure during the ablation [12], and the single phase anatase thin films were fabricated in 1.5×10^{-2} Torr. These samples were annealed in a vacuum or oxygen atmosphere for 10 to 60 min at 400˚C to 900˚C, for a total of 72 samples. XRD patterns of these samples were then acquired at 0.01 rad intervals. A He-Cd laser (λ = 325 nm) was used to measure the fluorescence intensity from the samples. If the spectrum of the XRD pattern is used as an input as it is, the explanatory variables exceed the prepared 72 samples and the risk of overfitting increases, so the number of explanatory variables should be reduced. For this reason, the peak positions and full width at half maximum (FWHM) data that commonly appeared in all the samples are shown in **Table 1** were extracted from

Table 1. Explanatory variables extracted from XRD.

Notation	Definition
P(101)	Peak position of (101)
P(103)	Peak position of (103)
P(004)	Peak position of (004)
P(112)	Peak position of (112)
P(200)	Peak position of (200)
P(105)	Peak position of (105)
P(211)	Peak position of (211)
F(101)	FWHM of (101)
F(103)	FWHM of (103)
F(004)	FWHM of (004)
F(112)	FWHM of (112)
F(200)	FWHM of (200)
F(105)	FWHM of (105)
F(211)	FWHM of (211)

the XRD patterns and used as explanatory variables. The integrated intensity of the luminescence of the ${}^4G_{5/2} \rightarrow {}^6H_{J/2}$ (J = 5, 7, 9, 11) inner shell transitions originating from Sm^{3+}, which was commonly observed in all samples, was calculated and the sum of them was used as the objective variable. These variables were tied together to construct a prediction model by LASSO regression. In LASSO model, the importance of each explanatory variable is expressed by the weight of that variable. These weights are chosen to minimize the following equation:

$$\sum_{i=1}^{N}\left(y_i - \beta_0 - \sum_{j=1}^{K}\beta_j x_j\right) + \alpha\sum_{j=1}^{K}\left|\beta_j\right| \tag{1}$$

where N is the number of samples, K is the number of explanatory variables, y_i is the true value of sample i, β_0 is the intercept, β_j is the weight of the j-th explanatory variable, and α is the tuning parameter.

3. Results and Discussion

Figure 1 shows the integrated PL intensity of the fluorescence from ${}^4G_{5/2} \rightarrow {}^6H_{J/2}$ (J = 5, 7, 9, 11) obtained from the PL measurement, normalized by the maximum value obtained in this experiment. The horizontal axis represents the temperature of the heat treatment applied to the material after film formation, and the vertical axis represents the time at which the temperature was maintained. Figure 1(a) shows the integrated luminescence intensity when the heat treatment was performed in an oxygen atmosphere. Figure 1(b) shows the integrated luminescence intensity when the heat treatment was performed in a vacuum, and the results are similar to those in Figure 1(a), but the integrated luminescence intensity is generally lower. Considering the relationship

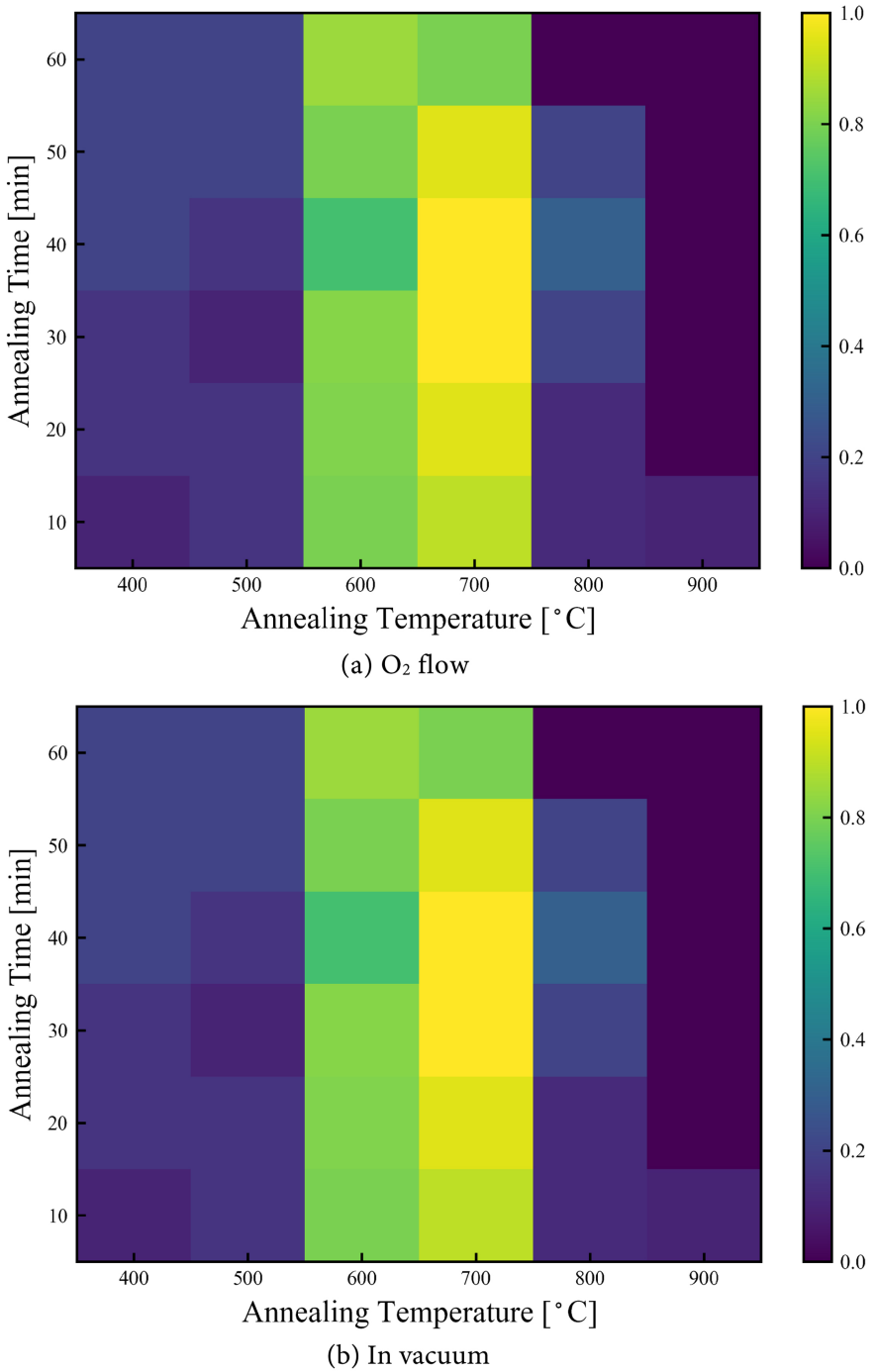

Figure 1. Integrated luminescence intensity normalized by the integrated luminescence intensity of a sample maintained at an annealing temperature of 700˚C for 40 minutes.

between (a) and (b) in **Figure 1**, it can be inferred that the presence or absence of oxygen defects plays a role. It is known that energy is exchanged between rare-earth ions in rare-earth doped phosphors, and the energy used for luminescence is lost with the increase of oxygen defects [17] [18], resulting in a decrease in the overall fluorescence intensity.

Figure 2 shows the lattice constants of the a- and c- axes calculated from the

XRD patterns using the Bragg equation. In this figure, a sample without annealing (As-depo in Figure 2) is prepared for comparison, and the average values of the lattice constants are plotted because the changes in the lattice constants were small at the same annealing temperature. From this figure, it can be seen that the annealing causes an overall decrease in the lattice constant compared to As-depo, and the decrease tends to increase with increasing annealing temperature.

As shown in Figure 3, the peak shifts and standard deviation of FWHM at the crystal plane were observed for all samples. Each point is derived from all the samples, which indicates that the peak shift varies from 0.02 rad to 0.07 rad among the samples. In contrast to the variation of the peak shift, the variation of the FWHM between samples is almost negligible.

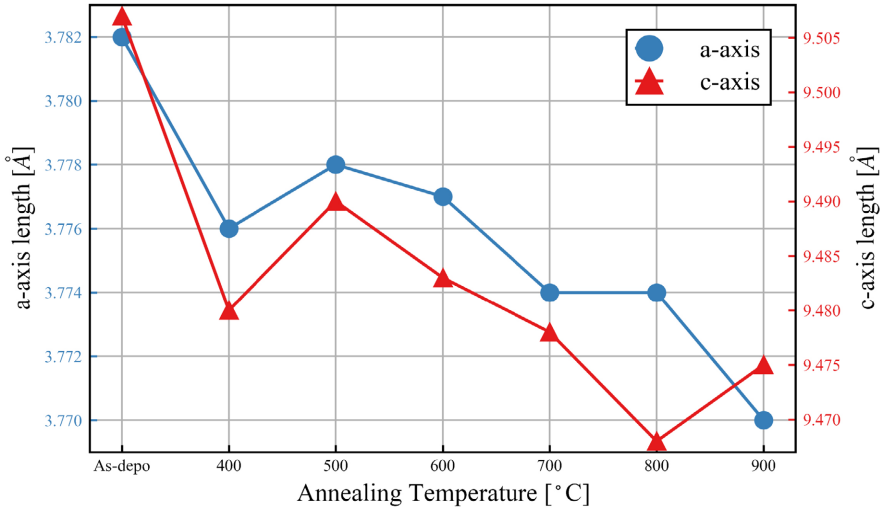

Figure 2. Variation of lattice parameter of a- and c-axis by annealing process.

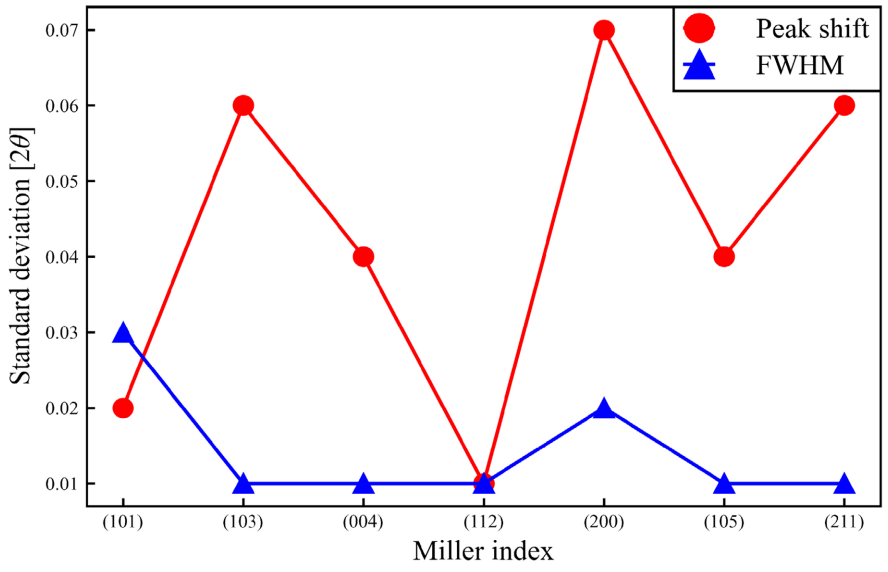

Figure 3. Distribution of peak shifts and FWHM variations in the crystal plane observed in XRD patterns of Sm-doped TiO_2 thin films.

Figure 4 shows the prediction results of the LASSO regression using the explanatory variables (Table 1) extracted from the XRD pattern. The coefficient of determination R^2 and the mean squared error (MSE) of this model were obtained to be 0.76 and 0.03, respectively. The closer the coefficient of determination is to 1, the better the fit of the model is, and the closer the MSE is to 0, the better the prediction is and with less error.

As shown in Figure 5, the importance of each explanatory variable estimated from the LASSO regression, excluding the explanatory variables that became zero because the LASSO regression sets parameters with low importance to zero. It

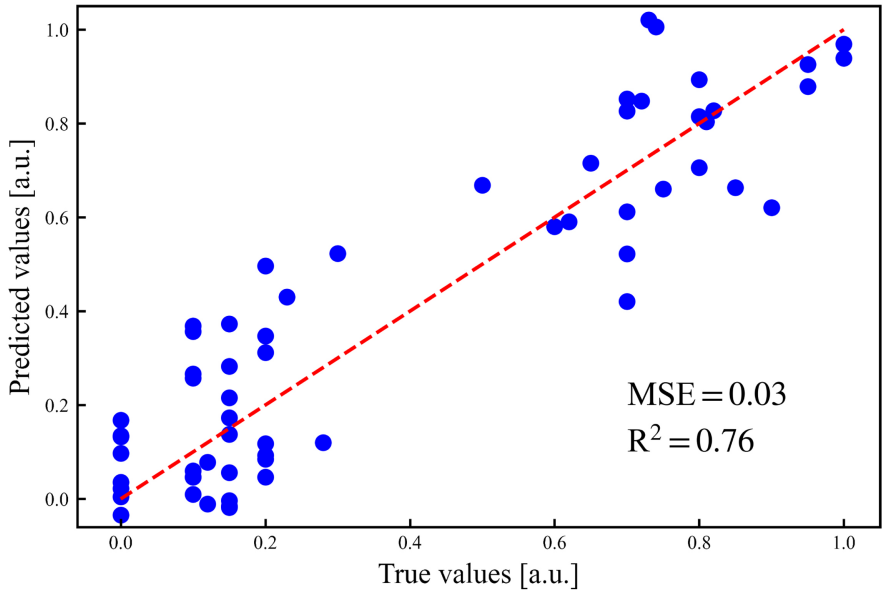

Figure 4. Relationship between luminescence integrated intensity predicted from LASSO regression and luminescence integrated intensity obtained from experiment.

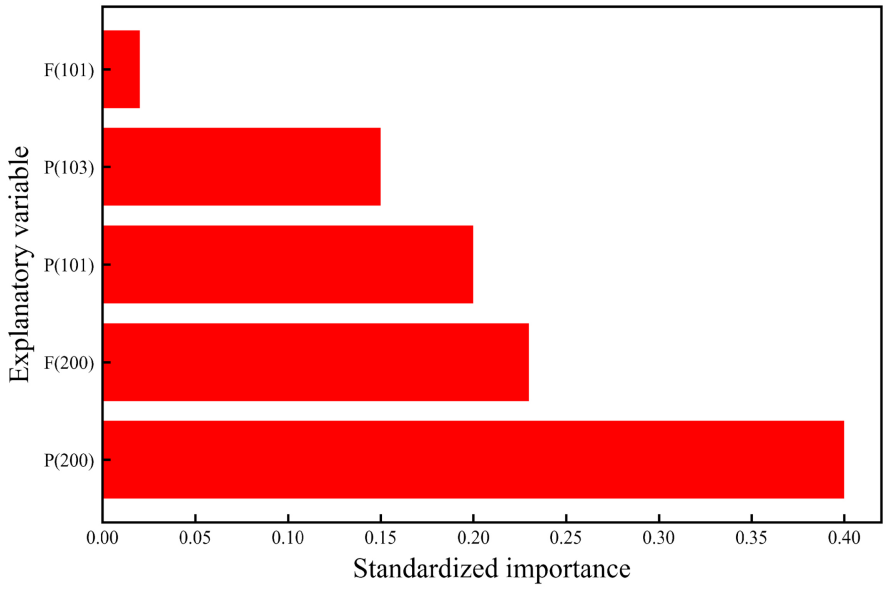

Figure 5. Importance of explanatory variables calculated from LASSO regression.

can be seen that the most important explanatory variables are P(200), F(200), P(101), P(103), and F(101) in that order. These important factors can be attributed to the incorporation of Sm into the matrix of TiO_2, which generates internal stresses [19], and furthermore, the incorporation of Sm changes the lattice constant as explained by Vegard's rule. Since the results of **Figure 2** show that the a- and c- axes change with increasing annealing temperature, it is considered that the increase in annealing temperature is proportional to the amount of Sm incorporated into the matrix of TiO_2. In this way, since the luminescence intensity is maximized at around 700˚C, it may be said that the internal stress generated by the Sm cells incorporated at around 700˚C created the local structure that maximizes the luminescence.

4. Conclusion

In this research investigation, the integrated luminescence of Sm-doped TiO_2 deposited on Si (100) substate in the visible light region is predicted by using XRD data. Since the raw XRD pattern has many data, we extracted the peak positions and half-widths of the peaks derived from TiO_2 and used these as explanatory variables. Using these explanatory variables and luminescence data, a model to predict the integrated luminescence intensity was constructed using LASSO regression, one of the machine learning algorithms. The model was able to predict the integrated luminescence intensity with high accuracy. It was found that P(200), F(200), P(101), P(103), and F(101) are important factors in this model. The background of this model is the incorporation of Sm into the matrix of TiO_2, which may express the relationship between the internal stresses generated by the incorporation and the local structure around Sm.

Acknowledgements

The authors would like to thank the member of Zhao laboratory for their experiment help and involvement in this study.

Conflicts of Interest

The authors declare no conflicts of interest regarding the publication of this paper.

References

[1] Zhou, B., Tao, L., Chai, Y., Lau, S.P., Zhang, Q.Y. and Tsang, Y.H. (2016) Constructing Interfacial Energy Transfer for Photon Up-and-Down-Conversion from Lanthanides in a Core-Shell Nanostructure. *Angewandte Chemie*, **128**, 12544-12548. https://doi.org/10.1002/ange.201604682

[2] Zhang, Z.L., Qin, J.Q., Shi, W.J., Liu, Y.Y., Zhang, Y., Liu, Y.F., Gao, H.P. and Mao, Y.L. (2018) Enhanced Power Conversion Efficiency of Perovskite Solar Cells with an Up-Conversion Material of Er^{3+}-Yb^{3+}-Li^{+} Tri-Doped TiO_2. *Nanoscale Research Letters*, **13**, Article No. 147. https://doi.org/10.1186/s11671-018-2545-y

[3] Fischer, S., Ivaturi, A., Krämer, K., Jakob, P., Martin-Rodriguez, R., Meijerink, A.,

Richards, B. and Goldschmidt, J. (2018) Upconversion Solar Cell Measurements Under Real Sunlight. *Optical Materials*, **84**, 389-395. https://doi.org/10.1016/j.optmat.2018.05.072

[4] Malathi, A., Madhavan, J., Ashokkumar, M. and Arunachalam, P. (2018) A Review on $BiVO_4$ Photocatalyst: Activity Enhancement Methods for Solar Photocatalytic Applications. *Applied Catalysis A*: *General*, **555**, 47-74. https://doi.org/10.1016/j.apcata.2018.02.010

[5] Khan, S., Parauha, Y., Halwar, D. and Dhoble, S. (2021) Rare Earth (RE) Doped Color Tunable Phosphors for White Light Emitting Diodes. *Journal of Physics: Conference Series*, **1913**, Article ID: 012017 https://doi.org/10.1088/1742-6596/1913/1/012017

[6] Hua, Y. and Yu, J. (2020) Photoluminescence Properties of Rare-Earth Ions-Activated Sr2YF7 Nanoparticles for WLED Devices. *Ceramics International*, **46**, 26646-26659. https://doi.org/10.1016/j.ceramint.2020.07.134

[7] Kumari, A., Soni, A. and Rai, V. (2016) Rare Earth Doped Upconverting Phosphors for Display and Temperature Sensing Applications. *Materials Focus*, **5**, 187-194. https://doi.org/10.1166/mat.2016.1328

[8] Binnemans, K. (2015) Interpretation of Europium(III) Spectra. *Coordination Chemical Reviews*, **295**, 1-45. https://doi.org/10.1016/j.ccr.2015.02.015

[9] Ishii, M., Komuro, S. and Morikawa, T. (2003) Study on Atomic Coordination Around Er Doped into Anatase-and-Rutile-TiO_2: Er-O Clustering Dependent on the Host Crystal Phase. *Journal of Applied Physics*, **94**, 3823-3827. https://doi.org/10.1063/1.1602567

[10] Aizawa, Y., Ohtuki, T., Harako, S., Komuro, S., Hirao, N. and Zhao, X. (2014) Sensitization Effect of Al Co-Doping on Nd-Related Photoluminescence in TiO_2 Matrix. *Japanese Journal of Applied Physics*, **53**, Article No. 06JG06. https://doi.org/10.7567/JJAP.53.06JG06

[11] Murayama, M., Yoda, K., Shiraishi, K., Guan, S., Komuro, S. and Zhao, X. (2018) Photoluminescence and Structural Analysis of Samarium Doped TiO_2 Thin Films and Their Applications to Visible LEDs. *Optics and Photonics Journal*, **8**, 146-164. https://doi.org/10.4236/opj.2018.85014

[12] Murayama, M., Yoda, K., Komuro, S., Crowe, I. and Zhao, X. (2019) Effect of Al Co-Doping on the Luminescence Properties of Nd^{3+}-Doped TiO_2 Thin Films. *Journal of Luminescence*, **216**, Article ID: 116656. https://doi.org/10.1016/j.jlumin.2019.116656

[13] Murayama, M., Yoda, K., Komuro, S., Nitani, H., Crowe, I. and Zhao, X. (2019) Influence of Al on the Local Structure of Nd-Doped TiO_2 Thin Films: A Combined Luminescence and X-Ray Absorption Fine Structure Analysis. *Materials Science and Engineering*: *B*, **246**, 49-52. https://doi.org/10.1016/j.mseb.2019.05.010

[14] Judd, B.R. (1962) Optical Absorption Intensities of Rare-Earth Ions. *Physical Review Journals Archive*, **127**, 750-761. https://doi.org/10.1103/PhysRev.127.750

[15] Ofelt, G.S. (1962) Intensities of Crystal Spectra of Rare-Earth Ions. *The Journal of Chemical Physics*, **37**, 511-520. https://doi.org/10.1063/1.1701366

[16] Tibshirani, R. (1996) Regression Shrinkage and Selection via the Lasso. *Journal of the Royal Statistical Society. Series B*, **58**, 267-288. https://doi.org/10.1111/j.2517-6161.1996.tb02080.x

[17] Devi, L.V., Selvalakshmi, T., Sellaiyan, S., Uedono, A., Sivaji, K. and Sankar, S. (2017) Effect of La Doping on the Lattice Defects and Photoluminescence Properties of CuO. *Journal of Alloys and Compounds*, **709**, 496-504.

https://doi.org/10.1016/j.jallcom.2017.03.148

[18] Yang, L.S., Li, G.S., Zhao, M.L., Yang, E.R. and Li, L.P. (2013) Lattice Defect Quenching Effects on Luminescence Properties of Eu^{3+}-Doped YVO_4 Nanoparticles. *Journal of Nanoparticle Research*, **15**, Article No. 1996. https://doi.org/10.1007/s11051-013-1996-4

[19] Yang, C.H. and Ma, Z.Q. (2012) Raman Spectral Analysis of TiO_2 Thin Films Doped with Rare-Earth Samarium. *Applied Optics*, **51**, 5438-5441. https://doi.org/10.1364/AO.51.005438